Short title:

Transmission of ROS signals from chloroplasts

Corresponding authors:

Andreas J. Meyer

Institute of Crop Science and Resource Conservation (INRES), Chemical Signalling,

University of Bonn

Friedrich-Ebert-Allee 144, D-53113 Bonn, Germany

Phone: +49 228 73 60353

Email: **andreas.meyer@uni-bonn.de**

Chloroplast-derived photo-oxidative stress causes changes in H_2O_2 and E_{GSH} in other subcellular compartments

Authors:

José Manuel Ugalde[1], Philippe Fuchs[1,2], Thomas Nietzel[2], Edoardo A. Cutolo[4], Ute C. Vothknecht[4], Loreto Holuigue[3], Markus Schwarzländer[2], Stefanie J. Müller-Schüssele[1], Andreas J. Meyer[1,*]

[1] Institute of Crop Science and Resource Conservation (INRES), University of Bonn, Friedrich-Ebert-Allee 144, D-53113 Bonn, Germany

[2] Institute of Plant Biology and Biotechnology, University of Münster, Schlossplatz 8, D-48143 Münster, Germany

[3] Departamento de Genética Molecular y Microbiología, Facultad de Ciencias Biológicas, Pontificia Universidad Católica de Chile, Avda. Libertador Bernardo O'Higgins 340, Santiago 8331150, Chile

[4] Institute of Cellular and Molecular Botany (IZMB), University of Bonn, Kirschallee 1, D-53115 Bonn, Germany

*Corresponding author: andreas.meyer@uni-bonn.de

One sentence summary: Methyl viologen-induced photooxidative stress causes an increase of H_2O_2 and oxidation of glutathione in chloroplasts, cytosol and mitochondria as well as autonomous oxidation in mitochondria.

Keywords: *Arabidopsis thaliana*, Methyl viologen, Glutathione redox potential, H_2O_2, Chloroplast, Mitochondria, Retrograde signaling, Interorganellar communication, Grx1-roGFP2, roGFP2-Orp1, Reactive oxygen species.

Footnotes:

Author contributions: J.M.U., U.C.V., L.H., S.J.M-S. and A.J.M. conceived and designed the experiments; J.M.U. performed the experiments; T.N. and E.A.C. contributed new constructs and plant lines; J.M.U., P.F., M.S., S.J.M.-S. and A.J.M. analyzed the data; J.M.U., S.J.M-S., and A.J.M. wrote the manuscript with contributions from all authors.

Funding information:

This work was supported by the Deutsche Forschungsgemeinschaft (DFG) through the Research Training Group GRK 2064 "Water use efficiency and drought stress responses: From Arabidopsis to Barley" (A.J.M.; M.S.; S.J.M.-S.; U.C.V.), grants ME1567/9-1/2 and SCHW719/7-1 within the Priority Program SPP1710 "Dynamics of thiol-based redox switches in cellular physiology" (A.J.M.; M.S.), the MSC-ITN project no. 607607 'CALIPSO' (U.C.V.; E.A.C.), grant MU 4137/1-1 (S.J.M.-S.) and the Emmy-Noether programme (SCHW1719/1-1; M.S.).

Present address: E.A.C.: Laboratory of Photosynthesis and Bioenergy, Department of Biotechnology, University of Verona, Verona, Strada le Grazie 15, 37134 Italy

Author for correspondence: andreas.meyer@uni-bonn.de

ABSTRACT

Metabolic fluctuations in chloroplasts and mitochondria can trigger retrograde signals to modify nuclear gene expression. Mobile signals likely to be involved are reactive oxygen species (ROS), which can operate protein redox switches by oxidation of specific cysteine residues. Redox buffers such as the highly reduced glutathione pool serve as reservoirs of reducing power for several ROS scavenging and ROS-induced damage repair pathways. Formation of glutathione disulfide (GSSG) and a shift of the glutathione redox potential (E_{GSH}) towards less negative values is considered a hallmark of several stress conditions. Here we used the herbicide methyl viologen (MV) to generate ROS locally in chloroplasts of intact Arabidopsis seedlings and recorded dynamic changes in E_{GSH} and H_2O_2 levels with the genetically-encoded biosensors Grx1-roGFP2 (for E_{GSH}) and roGFP2-Orp1 (for H_2O_2) targeted to chloroplasts, the cytosol or mitochondria. Treatment of seedlings with MV caused a rapid oxidation in chloroplasts and subsequently also in the cytosol and mitochondria. The MV-induced oxidation was significantly boosted by illumination with actinic light and largely abolished by inhibitors of photosynthetic electron transport. In addition, MV also induced an autonomous oxidation in the mitochondrial matrix in an electron transport chain activity-dependent manner that was milder than the oxidation triggered in chloroplasts by the combination of MV and light. *In vivo* redox biosensing resolves the spatiotemporal dynamics of compartmental responses to local ROS generation and provide a basis for understanding how compartment-specific redox dynamics may operate in retrograde signaling and stress acclimation in plants.

INTRODUCTION

Communication between different subcellular compartments of plant cells is fundamental to establish and sustain cooperative functioning and to acclimate to diverse environmental conditions. Since most plastidial and mitochondrial proteins are encoded in the nuclear genome, retrograde signals from the organelles to the nucleus are essential to adjust organelle function by coordinating the expression of nuclear and organellar genomes (Van Aken et al., 2016; de Souza et al., 2017; Dietz et al., 2019). Communication between the endosymbiotic organelles and the nucleus is likely to involve the cytosol as the intermediate compartment. However, chloroplasts can also make direct physical contact with the nuclear envelope via stromules, which has been suggested to mediate signaling (Caplan et al., 2015; Erickson et al., 2017; Exposito-Rodriguez et al., 2017). Physical interaction also occurs between different organelles and may facilitate efficient exchange of metabolites and information (Pérez-Sancho et al., 2016; Perico and Sparkes, 2018).

Reactive oxygen species (ROS), such as H_2O_2, have emerged as signaling molecules in plants and their roles in early signaling events initiated by cellular metabolic perturbation and environmental stimuli are established (Waszczak et al., 2018; Smirnoff and Arnaud, 2019). During unfavorable environmental conditions, superoxide ($O_2^{\bullet-}$) is produced at an increased rate by the electron transport chains (ETCs) in chloroplasts and mitochondria. $O_2^{\bullet-}$ is rapidly converted to hydrogen peroxide (H_2O_2) and molecular oxygen (O_2) by superoxide dismutases (SODs). H_2O_2 can be further detoxified through a set of peroxidases, including peroxiredoxins (PRX) (Liebthal et al., 2018)) several glutathione *S*-transferases (GST) (Sylvestre-Gonon et al., 2019; Ugalde et al., 2020), glutathione peroxidase-like enzymes (GPXL) (Attacha et al., 2017), and ascorbate peroxidases (APX). The latter operate as part of the glutathione–ascorbate cycle in the plastid stroma, mitochondrial matrix, peroxisomes and cytosol (Foyer and Noctor, 2005; Narendra et al., 2006). The transient drain of electrons from the local glutathione redox buffer causes a concomitant increase in glutathione disulfide (GSSG) and hence a change in the glutathione redox potential (E_{GSH}) (Marty et al., 2009; Bangash et al., 2019; Nietzel et al., 2019; Wagner et al., 2019). Intracellular H_2O_2 levels reached under stress conditions can affect cellular redox regulation leading to the oxidation of protein thiols (Dietz et al., 2016). H_2O_2 was shown to diffuse across the chloroplast envelope even at low concentrations, and it has been estimated that about 5% of the total ROS produced in high light leave the chloroplast (Mubarakshina et al., 2010). Those properties

contributed to the suggestion of H_2O_2 to operate as a messenger in signaling processes arising from the organelles. Moreover, direct transfer of H_2O_2 from a subpopulation of chloroplasts localized in close proximity to the nucleus itself was recently found to mediate photosynthetic control over gene expression in tobacco leaves (Caplan et al., 2015; Exposito-Rodriguez et al., 2017).

ROS production at specific sites of the photosynthetic ETC (pETC) can be artificially enhanced by using inhibitors and redox catalysts. Among these, the herbicide methyl viologen (MV) acts by re-directing electrons from photosystem I (PSI) to O_2 and thereby enhancing the production of $O_2^{\cdot-}$ (Scarpeci et al., 2008). Based on its mechanism, MV is also useful as an experimental cue to induce photo-oxidative stress in photosynthetic organisms. In mammals and other non-photosynthetic organisms, MV induces the generation of $O_2^{\cdot-}$ by re-directing electrons from complex I of the mitochondrial ETC (mETC) to O_2 (Cochemé and Murphy, 2008), suggesting that current models to study retrograde signaling are likely to be more complex than previously expected and involve additional subcellular sites (Cui et al., 2019; Shapiguzov et al., 2019). Steady-state measurements in cotyledons of Arabidopsis seedlings have previously shown that MV can induce oxidation in both cytosol and mitochondria in the absence of illumination (Schwarzländer et al., 2009).

Chemical probes for detecting ROS in living systems, such as 2',7'-dihydrodichlorofluorescein diacetate are typically converted to a fluorescent product through reaction with ROS and accumulate in tissues with different specificities for distinct forms of ROS (Fichman et al., 2019). While these dyes provide evidence for redox processes and ROS formation, a potential drawback is that those probes act irreversibly by generating an accumulative signal rather than a reversible, dynamic response. Further, their lack of unambiguous subcellular localization and chemical specificity make it frequently difficult to draw mechanistic conclusions. During the last decade, genetically encoded biosensors have revolutionized the field of cell physiology by being targetable to specific subcellular compartments and enabling dynamic measurements (Morgan et al., 2016). Among them, Grx1-roGFP2 for sensing E_{GSH} (Marty et al., 2009) and roGFP2-Orp1 for sensing transient changes in H_2O_2 (Nietzel et al., 2019); the latter being based on a redox relay between the H_2O_2-sensitive Gpx3 peroxidase from yeast (Orp1) and roGFP2 (Gutscher et al., 2009). These sensors have become instrumental to monitor the dynamics of oxidative signals in real-time in a wide range of organisms, including plants. Similarly, probes of the HyPer family,

which exploit the H_2O_2-sensitive bacterial transcription factor OxyR for their response, can report on local alterations in H_2O_2 concentrations (Bilan and Belousov, 2018; Pak et al., 2020).

Despite compelling evidence for the signaling functions of H_2O_2, it is neither known how H_2O_2 concentrations and the redox buffers dynamically respond to increased ROS production in chloroplasts nor how much other organelles contribute to a cumulative oxidation in the cytosol. Here, we targeted two different roGFP2-based biosensors to the stroma of the chloroplasts, the cytosol and the matrix of the mitochondria to live monitor the local E_{GSH} and H_2O_2 dynamics specifically in those three compartments. We investigated the dynamic subcellular responses to primary oxidative events triggered by MV, light or a combination of both. To dissect the contribution of chloroplasts and mitochondria in the MV-induced overall oxidation, the respective ETCs were blocked using ETC-specific inhibitors acting at early steps of electron transport.

RESULTS

Spectral properties of roGFP2-based probes *in planta*

To visualize changes of E_{GSH} or H_2O_2 levels in chloroplasts, cytosol and mitochondria, we selected previously published Arabidopsis reporter lines with roGFP2 linked to Grx1 or Orp1, respectively (Marty et al., 2009; Park et al., 2013; Albrecht et al., 2014; Nietzel et al., 2019). Since no roGFP2-Orp1 reporter line for H_2O_2 sensing in the plastid was available, we generated this line *de novo* (Supplemental Fig. S1). Subcellular localization of all reporter constructs was verified side-by-side in 7-day-old seedlings by confocal microscopy (Fig. 1A–F, left panels and Supplemental Fig. S1). Plants of the same age were used to systematically corroborate the *in vivo* excitation spectra of both redox sensors in all three compartments of intact seedlings. Sensor response and the dynamic spectroscopic response range was assessed by recording the fluorescence of seedlings immersed in imaging buffer using a fluorescence multiwell plate reader. Fluorescence spectra were collected for non-treated seedlings and seedlings incubated with either 20 mM DTT for complete reduction or with 100 mM H_2O_2 for complete oxidation of the sensors *in situ* (Fig. 1A–F, right panels). Sensor fluorescence intensities were sufficiently high to be clearly distinguishable from background fluorescence with a suitable signal-to-noise ratio for *in situ* readings (Supplemental Fig. S2). Fully reduced Grx1-roGFP2 (roGFP2-Grx1 in the case of the mitochondria) or roGFP2-Orp1 showed low excitation at 400 nm and a pronounced excitation peak close to 488 nm in all compartments. Probe oxidation led to the appearance of a second distinct excitation peak close to 400 nm, while excitation at 488 nm was decreased (Fig. 1A–F, right panels, Supplemental Fig. S2). The spectral behavior of both probes *in planta* was consistent with the spectra of the purified roGFP2 *in vitro* (Fig. 1H). These data validate that changes in the redox state of both roGFP2-based sensor variants can be reliably visualized and recorded in chloroplast stroma, cytosol and mitochondrial matrix using plate reader-based fluorimetry (Nietzel et al., 2019; Wagner et al., 2019).

Real-time monitoring of E_{GSH} and H_2O_2 dynamics in Arabidopsis in response to externally imposed oxidative stress

To further validate the responsiveness of both probes *in planta,* 7-day-old Arabidopsis seedlings expressing cytosol-targeted Grx1-roGFP2 or roGFP2-Orp1 were exposed to different concentrations of H_2O_2 to impose oxidative stress (Fig. 2A, B). Changes in the

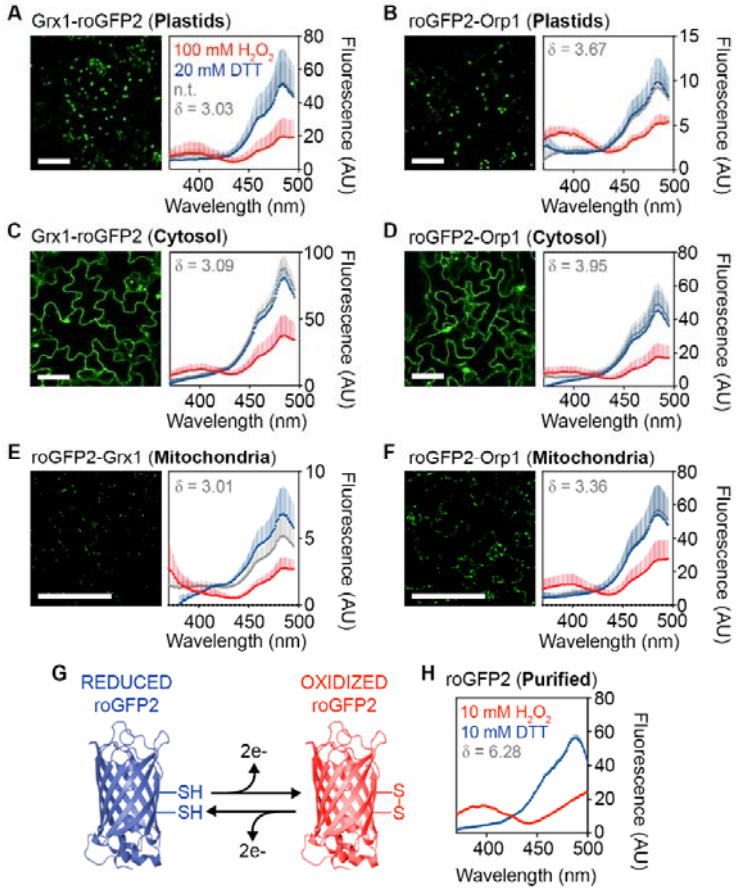

Figure 1. Subcellular localization and spectral behavior of E_{GSH} and H_2O_2 sensors in Arabidopsis. **A–F (left panels)**, Confocal microscopy images of leaf epidermal cells from 7-day-old seedlings stably expressing Grx1-roGFP2, roGFP2-Grx1 or roGFP2-Orp1 targeted to plastids (**A–B**), cytosol (**C–D**) or mitochondria (**E–F**). All images show roGFP2 fluorescence recorded with λex = 488 nm and λem = 505-530 nm. Bars, 50 µm. **A–F (right panels)**, Grx1-roGFP2, roGFP2-Grx1 or roGFP2-Orp1 fluorescence excitation spectra for non-treated seedlings (n.t., grey), and after reduction with 20 mM DTT (blue) or oxidation with 100 mM H_2O_2 (red). All spectra were recorded on a plate reader from 7-day-old seedlings with emission at 520±5 nm and using the same gain for all lines. The curves show the mean of the fluorescence in arbitrary units (AU) +SD, with n ≥ 3 biological replicates, where each replicate is an independent pool of 4–5 seedlings. All spectra were corrected for the autofluorescence measured in non-transformed control seedlings (see Supplemental Fig. S1). The dynamic range (δ) for the maximum change of the fluorescence ratio between the fully oxidized and fully reduced sensor was calculated from the fluorescence collected after sensor excitation at 410 and 480 nm. **G**, Schematic model of roGFP2 structure highlighting the disulfide bond formation upon reversible oxidation. **H**, Excitation spectrum of purified roGFP2 measured under similar conditions as the seedlings. To achieve full reduction and full oxidation, the purified protein was incubated in 10 mM DTT or 10 mM H_2O_2, respectively. Mean +SD, n = 6.

178 redox state of both sensors were followed in real-time by exciting roGFP2 at 410 nm and 480
179 nm (Fig. 2B, C, E). The recorded fluorescence of roGFP2 in the individual channels (410 and
180 480 nm) showed an immediate response in opposite directions upon addition of H_2O_2, with a

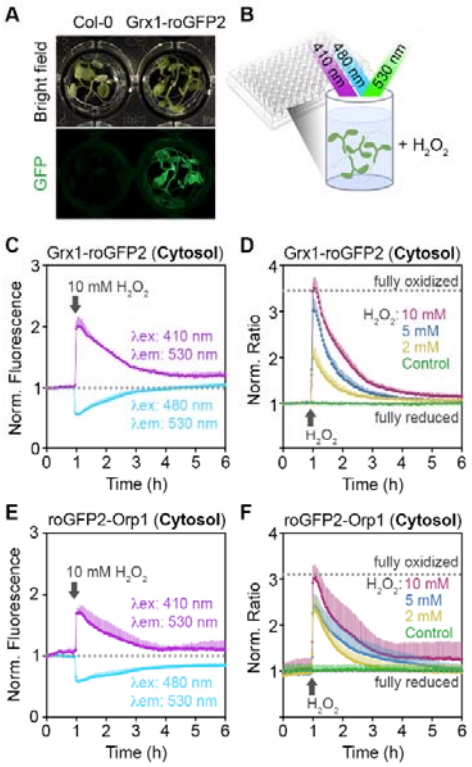

Figure 2. Real-time monitoring of cytosolic Grx1-roGFP2 and roGFP2-Orp1 redox changes upon imposition of oxidative stress *in planta*. **A**, Pools of 7-day-old seedlings (4–5 per well) expressing Grx1-roGFP2 or roGFP2-Orp1 in the cytosol were placed in a 96-well plate. **B**, The redox state of the sensors was measured as the roGFP2 fluorescence after sequential excitation at λex = 410±5 nm and λ ex = 480±5 nm. Fluorescence was always recorded at λem = 530±20 nm. **C**, **E**, Time–resolved fluorescence recordings for the two independent channels after addition of 100 mM H_2O_2 at t = 1 h. Both curves are normalized to their initial values before imposed oxidation (dotted lines). **D**, **F**, Fluorescence ratio values calculated to the original fluorescence in both channels in response to different concentrations of H_2O_2. For control samples only buffer was added. The curves show the mean ratio +SD from n = 4 biological replicates, where each replicate is an independent pool of 4–5 seedlings. The ratio values are normalized to the original ratio values before addition of H_2O_2. The experiment was repeated three times with similar results. Dotted lines in panels D and F indicate minimum and maximum ratio values measured from the same wells at the end of the experiment during incubation in 100 mM H_2O_2 for full oxidation and in 20 mM DTT for full reduction of the probes (see Supplemental Fig. S3).

181 increase of the 410 nm channel while the fluorescence excited at 480 nm decreased (Fig. 2C,
182 E; Supplemental Fig. S3A-E). After reaching a peak of oxidation, a gradual recovery of both
183 channels towards the starting values occurred over a period of about four hours (Fig. 2C, E,

Supplemental Fig. S3). For analysis, the 410 nm/480 nm fluorescence ratio was calculated and used as a measure for sensor oxidation (Fig. 2D, F). Starting from low ratio values in non-treated seedlings the addition of H_2O_2 caused a rapid increase of the 410 nm/480 nm fluorescence ratio. While the speed of oxidation was independent of the amount of H_2O_2, the maximum peak height increased with increasing concentrations of H_2O_2 (Fig. 2D, F). In all experiments, the minimum and maximum fluorescence ratios of the respective probes in their fully oxidized and fully reduced state were determined after each experiment as shown for the cytosolic roGFP2-Orp1 sensor (Supplemental Fig. S3F).

The dominant impact of MV-induced glutathione oxidation occurs in the chloroplasts

After confirming the fast and concentration-dependent response of the sensors towards H_2O_2 treatments *in vivo*, we evaluated the sensitivity of the plate reader-based fluorimetry setup to detect redox changes induced by MV. For this purpose, 7-day-old seedlings expressing Grx1-roGFP2, roGFP2-Grx1 or roGFP2-Orp1 targeted to plastid stroma, the cytosol or the mitochondrial matrix were treated with different concentrations of MV and sensor fluorescence was continuously recorded in plate reading mode for 6 h (Fig. 3). In chloroplasts, the oxidation of both probes gradually increased over time, with roGFP2-Orp1 showing a faster oxidation immediately after MV treatments compared to Grx1-roGFP2 (Fig. 3A–C; Supplemental Fig. S4A–B). In contrast to the response in chloroplasts, the fluorescence ratios of cytosolic Grx1-roGFP2 and roGFP2-Orp1 remained low suggesting that both probes remained largely reduced under the same treatments (Fig. 3D–F). Despite the slow oxidation, ratio values five hours after addition of MV were higher than in control seedlings. . In mitochondria both sensors revealed a gradual oxidation after the addition of 100 µM MV, roGFP2-Orp1 ratio increased more strongly during the first five hours after the addition of MV than roGFP2-Grx1(Fig. 3G–I). Because the action of MV in chloroplast is light-dependent, we further tested whether the flashes of light used for roGFP2 excitation were sufficient to cause the oxidation of roGFP2 by photooxidation effects. Increasing the cycle time of fluorescence readings from individual wells from 3 to 60 min abolished the detectable roGFP2-Orp1 oxidation in chloroplasts and the cytosol, which is consistent with light-dependency of MV-mediated ROS generation in chloroplasts (Supplemental Fig. S5). In mitochondria, the oxidation five hours after addition of MV was also visible albeit to a lower extent than with high flash frequencies. The steady increase of the fluorescence ratio with high repetition rates for the readout (Fig. 3) suggests that the oxidation effect caused by the

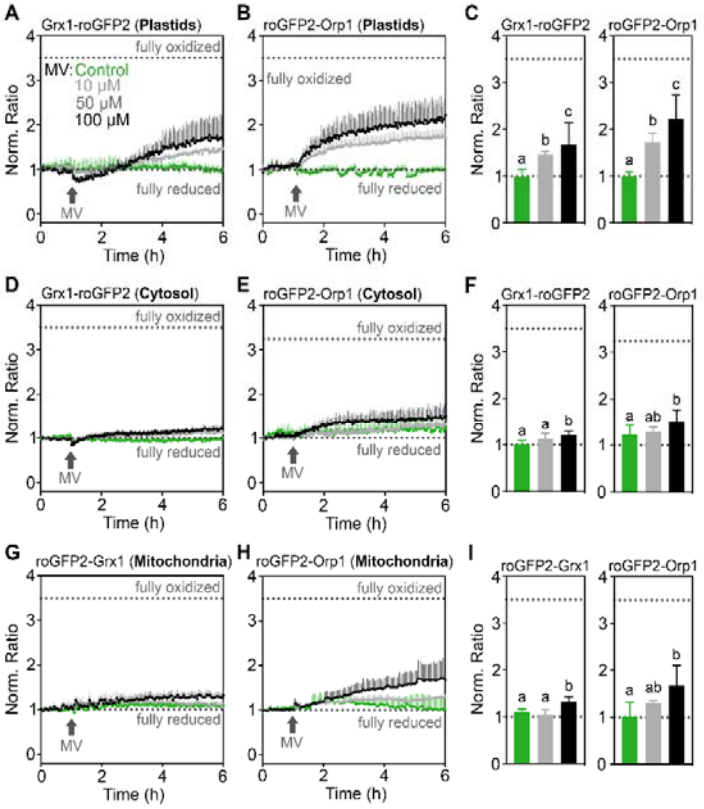

Figure 3. Real-time monitoring of E_{GSH} and H_2O_2 sensors upon MV-induced oxidation *in planta*. **A–I**, Seven-day-old seedlings stably expressing Grx1-roGFP2, roGFP-Grx1 or roGFP2-Orp1 targeted to the cytosol, plastids or mitochondria were placed in a 96-well plate with imaging buffer. After 1 h, MV was added to a final concentration indicated in panel A. In control samples (green), only buffer was added to maintain a uniform total buffer volume throughout the experiments. Ratio values were calculated from the fluorescence recorded by sequential excitation of probes at 410±5 nm and 480±5 nm, and normalized to the initial ratio at 0 h. Fluorescence was always recorded at 530±20 nm. Dotted lines indicate ratio values measured from the same wells at the end of each experiment after incubation in 20 mM DTT for full reduction or 100 mM H_2O_2 for full oxidation of the probes. **C**, **F**, **I**, Endpoint ratio values at 6 h extracted from panels A, B, D, E, G and H. Mean ratios +SD, n ≥ 3 biological replicates, where each replicate is an independent pool of 4–5 seedlings. Different letters indicate statistical differences between ratios after log10 transformation, according to one-way ANOVA with Tukey's multiple comparison test ($P < 0.05$). Data for individual excitation channels are presented in Supplemental Fig. S4.

herbicide is not reversible and exceeds the endogenous reducing capacity. The pronounced increase in the fluorescence ratio for both sensors targeted to chloroplast and mitochondria in response to 100 µM MV suggests that a local increase of H_2O_2 occurs in these organelles

(Supplemental Fig. S4A–B), implying that the oxidation of the chloroplastic glutathione pool exceeds the oxidation measured in the cytosol and in mitochondria and that the light flashes used to excite the fluorophore enhance the MV-induced oxidation.

Continuous light enhances MV-induced oxidation in chloroplasts, cytosol and mitochondria

The more pronounced oxidation induced by MV in chloroplasts compared to the cytosol and mitochondria (Fig. 3) was related to the unavoidable intermittent illumination during data collection (Supplemental Fig. S5). While this primary oxidation in chloroplasts was exploited for the following experiments, the results would only be physiologically meaningful as long as the seedlings do not get seriously damaged over the course of the experiment, especially when illuminated at high frequencies or even intermittent periods of continuous light. To test whether MV in combination with illumination had obvious effects on plant viability, Arabidopsis seedlings that had been exposed to excitation light every three minutes for a 15 hour fluorescence recording were taken out of the plates and transferred to agar plates for phenotype documentation. All seedlings that had been repeatedly illuminated with excitation light were still green and fully turgescent irrespective of the MV concentration (Supplemental Fig. S6A). Even if seedlings were illuminated with constant actinic light with an intensity of 200 µmol m^{-2} s^{-1} for 1 h after the first 2 hours of the 15 h time course, no obvious toxic effect of MV could be recognized macroscopically (Supplemental Fig. S6B). By contrast, seedlings kept under constant actinic light with an intensity of 200 µmol m^{-2} s^{-1} for 15 h showed loss of chlorophyll already with 10 µM MV and even more seriously with 100 µM MV, which caused complete bleaching (Supplemental Fig. S6C).

After confirming that 1 h illumination outside the plate reader does not severely damage the seedlings, we used this regime to further boost ROS formation in chloroplasts (Fig. 4A–I). The 1-hour illumination with constant actinic light with an intensity of 200 µmol m^{-2} s^{-1} caused a transient increase in the fluorescence ratio of both sensors targeted to chloroplasts and mitochondria in untreated control seedlings (Fig. 4A–B, G–H, green curves). For technical reasons, resuming roGFP measurements after intermittent illumination of seedlings outside the plate reader was only possible after a lag time of about 10 seconds post-illumination, since the plates needed to be transferred back into the reader. Conversely, the sensors in the cytosol in control plants did not respond to illumination alone (Fig. 4D–E, green lines). The combination of MV and illumination, however, induced an increase in the

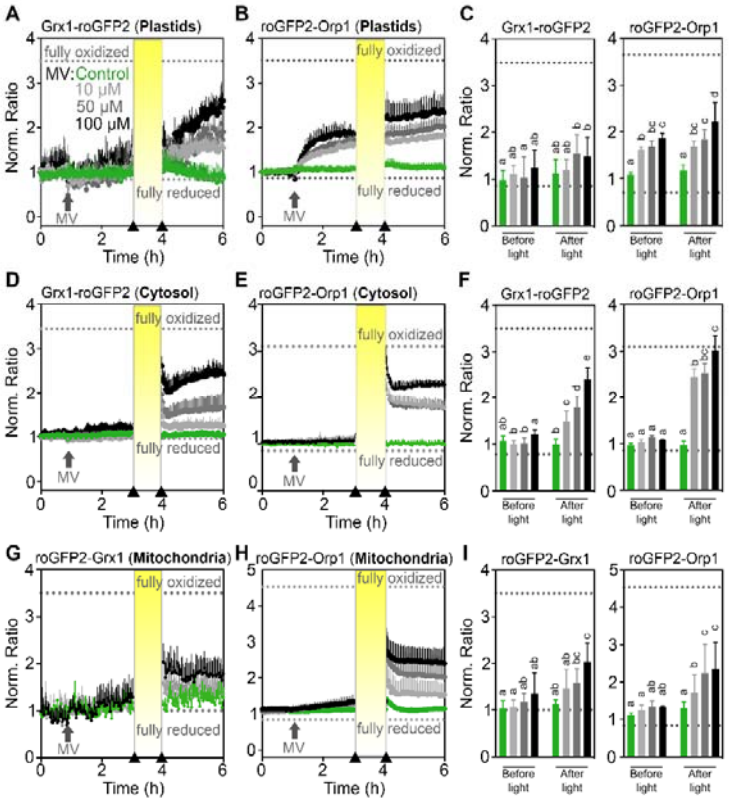

Figure 4. Light enhances MV-induced oxidation of roGFP2-derived redox sensors. A–I, Seven-day-old seedlings stably expressing the indicated sensor constructs in plastids, in the cytosol or in mitochondria were placed in a 96-well plate with imaging buffer. After 1 h, MV was added to final concentrations of indicated in panel A. Arrows on the x-axes of panels A, B, D, E, G, and H indicate the time points at which data for the bar charts in panels **C**, **F** and **I** were extracted (i.e. before and after illumination). In control samples (green), only buffer was added. Oxidation of the sensors was recorded as the normalized ratio of the fluorescence recorded with excitation at 410±5 nm and 480±5 nm, respectively. Fluorescence was always recorded at 530±20 nm. After a pre-incubation with MV for 2 h, seedlings were intermittently illuminated for 1 h with actinic light (200 µmol m^{-2} s^{-1}) and redox measurements were subsequently resumed for 2 h. Dotted lines indicate ratio values measured from the same wells at the end of the experiment after incubation in 20 mM DTT for full reduction or 100 mM H2O2 for full oxidation of the probes. Mean ratios +SD, n ≥ 4 biological replicates, where each replicate is an independent pool of 4–5 seedlings. Different letters represent statistical differences between ratios after log10 transformation, according to one-way ANOVA with Tukey's multiple comparison test ($P < 0.05$). Data for individual channels can be found in Supplemental Fig. S7.

251 fluorescence ratio for both sensors in all three compartments, resulting in a transitory peak of
252 oxidation lasting close to 10 minutes after illumination. The long-term measurement shows a
253 gradual oxidation over time (Fig. 4). This oxidation was dependent on the concentration of

MV applied, albeit with different amplitudes depending on the probe and on the compartment. While Grx1-roGFP2 in the cytosol showed a pronounced long-term ratio increase in plants pre-incubated with 50 and 100 µM MV, the ratio change of cytosolic roGFP2-Orp1 was limited to a minor reversible increase only (Fig. 4D–F). In mitochondria, light exposure caused transient oxidation of roGFP2-Orp1 and roGFP2-Grx1 albeit without pronounced differences between the two probes (Fig. 4G–I).

Chloroplasts and mitochondria contribute to MV-induced oxidative stress

Flash illumination for roGFP2 fluorescence measurements during plate reader-based fluorescence excitation with intervals of 1 h did not lead to changes in roGFP2 fluorescence ratios in chloroplasts and the cytosol (Supplemental Fig. S5B). In mitochondria, however, the fluorescence ratio did show a small increase pointing at the possibility of an autonomous mitochondrial oxidative response, which was also recently concluded by independent work using orthogonal approaches (Cui et al., 2019). To dissect the relative contributions of chloroplasts and mitochondria to the MV-induced oxidative response in the cytosol, we used inhibitors for the two different ETCs. Seedlings expressing the different sensors were pre-treated with either 3-(3,4-dichlorophenyl)-1,1-dimethylurea (DCMU) to inhibit the electron transport between PSII and plastoquinone, or rotenone to inhibit the mETC at complex I (Fig. 5A–B). DCMU pre-treatment decreased MV-induced oxidation of both plastid-targeted sensors compared to seedlings treated with MV alone (Fig. 5C, dark green and black curves). The inhibitory effect of DCMU was most evident immediately after illumination in seedlings expressing Grx1-roGFP2. In seedlings expressing roGFP2-Orp1, DCMU inhibited the oxidation of the sensor as well, albeit to a lesser extent. Inhibition of the pETC by DCMU also inhibited the light-induced oxidation of the cytosolic Grx1-roGFP2 (Fig. 5E) and mitochondrial roGFP2-Grx1 (Fig. 5G, left panel). At the same time the fluorescence ratio increase of mitochondrial roGFP2-Orp1 was restricted to about 50–70% by DCMU (Fig. 5G, right panel). Pre-treatments with rotenone noticeably suppressed the illumination- and MV-induced ratio increase of Grx1-roGFP2 in chloroplasts and cytosol (Fig. 5D, F, left panels, dark red and black curves). The inhibitory effect of rotenone, however, was less pronounced than that of DCMU (Fig. 5C, E, left panels).

By contrast, roGFP2-Orp1 targeted to the plastids and the cytosol were not affected by incubation with rotenone (Fig. 5D, F, right panels). Rotenone pre-treatment on plants expressing the two sensors in mitochondria showed minor inhibition of the MV-induced ratio

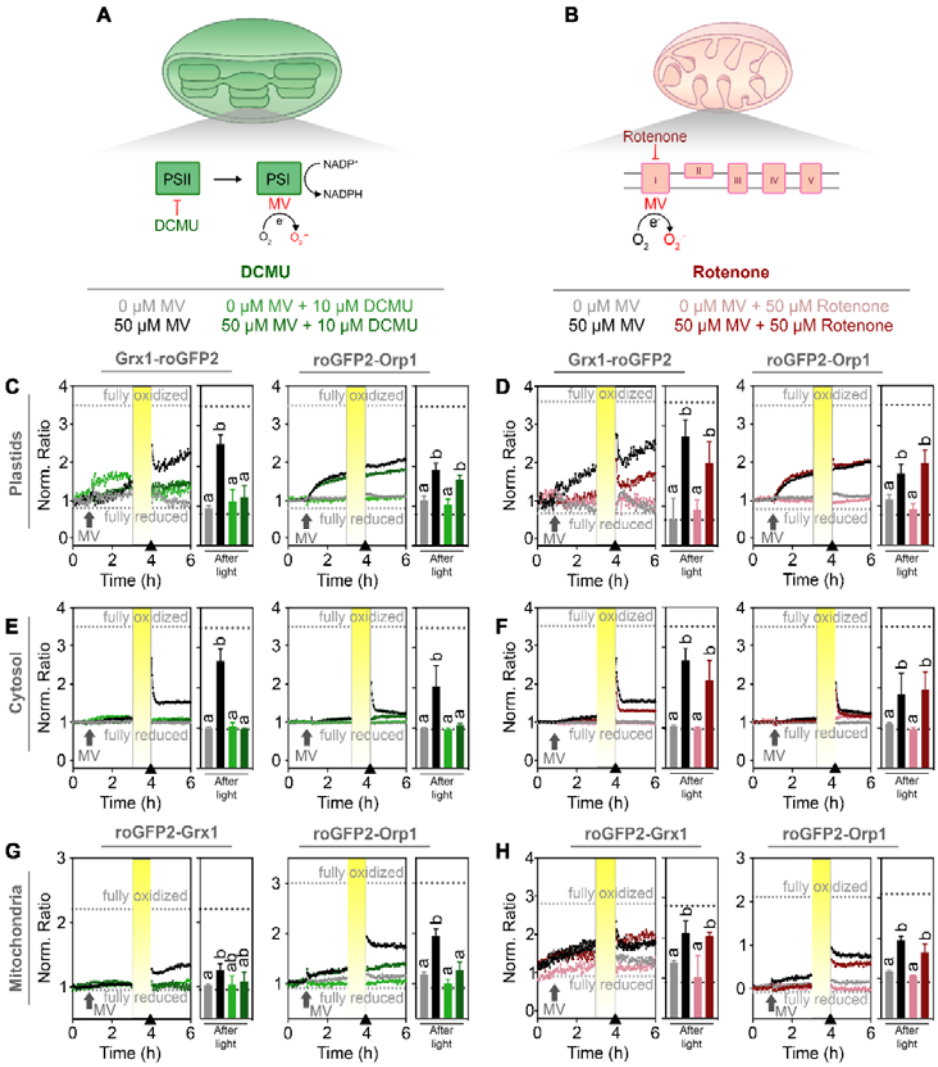

Figure 5. Contribution of chloroplast and mitochondrial ETCs to MV-induced oxidation. A, Model depicting the function and interplay of MV and ETC inhibitors on superoxide production in a chloroplast. MV withdraws electrons (e-) from photosystem I (PSI) and transfers them to molecular oxygen (O_2) to form superoxide ($O_2^{\bullet-}$). DCMU is an inhibitor that specifically blocks electron transfer from photosystem II (PSII) to plastoquinone. **B**, In the mitochondrion, MV is able to transfer electrons from complex I of the mitochondrial electron transport chain to O_2, generating $O_2^{\bullet-}$. Rotenone inhibits complex I activity. **C–H**, Seven-day-old seedlings stably expressing the indicated sensor constructs in plastids, cytosol or mitochondria were placed in 96-well plates with imaging buffer as a control or buffer supplemented with 10 µM DCMU or 50 µM rotenone to inhibit the electron flux along the chloroplastic or mitochondrial ETCs, respectively. After 1 h, MV was added to a final concentration of 50 µM or buffer as a control. After 2 h of treatments, the samples were intermittently exposed to 1 h of actinic light (200 µmol m^{-2} s^{-1}). Data indicate the mean normalized ratio of the sensor fluorescence sequentially excited at 410±5 nm and 480±5 nm, and collected at 530±20 nm in at least four biological replicates (left panels). Arrows on the x-axes of panels C–H indicate the time point at which data for the bar charts (right panels). Dotted lines indicate ratio values measured from the same wells at the end of the experiment during incubation in 20 mM DTT for full reduction or 100 mM H_2O_2 for full oxidation of the probes. Different letters represent statistical differences between ratios after log10 transformation, according to one-way ANOVA with Tukey's multiple comparison test ($P < 0.05$).

286 increase after illumination, particularly for the fluorescence ratio of roGFP2-Orp1 (Fig. 5H).
287 Immediately upon addition of MV to seedlings, a slight oxidation of the sensor in both
288 chloroplasts and mitochondria occurred independently of the illumination treatment (Fig. 5C,

289 D, G, H). The oxidation was still visible in chloroplasts and mitochondria of seedlings pre-
290 treated with DCMU, but was less pronounced in seedlings pre-treated with rotenone (Fig.
291 5H). This confirms that the pETC largely contributes to the light-induced oxidation of all
292 three compartments, while the mETC contributes only to a minor extent after illumination.

293

DISCUSSION

Dynamic recording of oxidative processes in multiple subcellular compartments of plant tissues using plate reader-based fluorimetry

Redox-sensitive GFPs have paved the way to elucidate the distinct differences in local E_{GSH} of subcellular compartments in plant cells (Jiang et al., 2006; Meyer et al., 2007; Schwarzländer et al., 2008). While roGFP2-based sensors for E_{GSH} are highly robust and reliable, sensor constructs for H_2O_2 monitoring are more diverse and exhibit a combination of integrated features (Schwarzländer et al., 2016). Probe variants of the HyPer family have been used multiple times in different subcellular compartments (Costa et al., 2010; Boisson-Dernier et al., 2013; Exposito-Rodriguez et al., 2017; Rodrigues et al., 2017; Mangano et al., 2018). Because HyPer is based on a circular permuted YFP a cleft in the artificial barrel structure allows direct access of protons to the central chromophore rendering most HyPer probes highly sensitive to pH, a feature that could potentially cause major artefacts in light-dependent measurements in chloroplasts (Belousov et al., 2006; Schwarzländer et al., 2014). An updated version, HyPer7, has been proven to be pH insensitive, but has not yet been used in plant research (Pak et al., 2020). Fusions of roGFP2 with peroxidases like the glutathione peroxidase Orp1 or peroxiredoxins, such as Tsa2 overcome this limitation because the roGFP2 ratio is pH-insensitive over the whole physiological range (Schwarzländer et al., 2008; Gutscher et al., 2009; Morgan et al., 2016). Orp1 fused to roGFP2 was chosen in this work based on its sensitivity to low H_2O_2 levels (Delaunay et al., 2002; Sobotta et al., 2013), its pH-insensitivity, and its dependence on reduction via Grx and GSH (Nietzel et al., 2019).

Environmental stress conditions can trigger oxidative processes via ROS formation. However, oxidation occurs with different dynamics and amplitudes in different subcellular compartments (Schwarzländer et al., 2009; Rosenwasser et al., 2011; Bratt et al., 2016). Dynamic measurements after triggering oxidative stress have been successfully carried out in the cytosol and mitochondria of cells and tissues placed in perfusion chambers on fluorescence microscopes (Schwarzländer et al., 2009). While high throughput approaches are limited in a typical microscopy set-up, plate reader-based approaches have enabled dynamic long-term measurements with multiple parallel samples in one experiment (Rosenwasser et al., 2010; Rosenwasser et al., 2011; Bratt et al., 2016; Nietzel et al., 2019; Wagner et al., 2019). Comparative measurements with Grx1-fused roGFP2 for E_{GSH} and roGFP2-Orp1 for H_2O_2 sensing recently revealed differential responses of both probes in the

cytosol and the mitochondrial matrix (Nietzel et al., 2019). Our results show that this approach can be extended to the chloroplasts, as the predominant generators of ROS under illumination (Mubarakshina et al., 2010).

While genetically encoded biosensors can be powerful tools for *in vivo* monitoring of physiological parameters, potential problems caused by overexpression, mis-targeting or incomplete targeting have been observed (Albrecht et al., 2014; De Col et al., 2017). In contrast to a slight developmental delay that we observed previously for Arabidopsis plants with mitochondrial roGFP2-Orp1 (Nietzel et al., 2019), Grx1-roGFP2 and roGFP2-Orp1 can both be targeted to plastids without any mis-targeting and without causing any apparent developmental phenotype. The absence of obvious phenotypes suggests that the reporter constructs and their import do not interfere with normal plastid functions. In microscopic experiments with high spatial resolution incomplete targeting may not pose a major problem or can even be exploited as an advantageous feature for simultaneous recording of physiological responses in two compartments (Marty et al., 2019). As we employ plate reader assays in which only the overall fluorescence from a biological sample is recorded, correct targeting of the probes to all compartments is of utmost importance and was carefully validated.

Previous reports using roGFP-based sensors have demonstrated a fast and reversible oxidation in response to external H_2O_2 (Meyer et al., 2007; Morgan et al., 2011). We observed similar fast oxidation kinetics for both tested sensors in the cytosol of Arabidopsis seedlings. 10 mM H_2O_2 were sufficient to reach the maximum oxidation of the sensors. This maximum oxidation, however, was not maintained but rather followed by an immediate recovery towards the fully reduced state over the course of five hours. This decrease in the fluorescence ratios of roGFP2 after severe oxidative challenge indicates a decrease of intracellular H_2O_2 and re-reduction of the cytosolic glutathione buffer, respectively. This recovery shows the remarkable efficiency of the plant peroxide detoxification machinery, enabling 4-5 seedlings with a total fresh weight of ~15 mg to clear a total volume of 200 µL from 10 mM H_2O_2 within five hours. This would amount to an average detoxification of about 440 nmol $(g\ FW)^{-1}\ min^{-1}$, which interestingly is in the order of 50-5,000 nmol $(g\ FW)^{-1}$ that has been reported for the H_2O_2 content in unstressed leaves (Queval et al., 2008). Although it is not the focus of this study, our experimental setup thus appears well suited for further genetic dissection of cellular peroxide detoxification systems (Smirnoff and Arnaud,

2019). The transitory peak for the maximum oxidation also highlights the need for immediate measurement of complete sensor oxidation for calibration purposes (Schwarzländer et al., 2008).

Real-time monitoring of MV-induced oxidative stress

While both roGFP2-based probes used here show an oxidative response after MV treatment within hours, it is already known that exposure of plants to MV triggers distinct changes in gene expression. In cucumber, MV causes the accumulation of ROS and lipid peroxides after 1 h, while GSH oxidation and an increase in ascorbate peroxidase (APX) and glutathione peroxidase (GPX) activities were identified 48 h after MV application (Liu et al., 2009). Light acts as an enhancer of the MV-induced oxidation, but is not essential for MV-induced oxidative damage (Cui et al., 2019; Shapiguzov et al., 2019).

Plants frequently contain a broad range of autofluorescent endogenous compounds (Müller et al., 2013). Reliable interpretation of sensor responses thus depends on correct recording and subtraction of such signals underlying and potentially obscuring the true roGFP2 signal (Fricker, 2016). While for short-term treatments with oxidative changes induced by light and/or MV this can be done reliably and additionally controlled for by careful monitoring the raw data for each individual channel, deviations in long-term measurements cannot be fully excluded. For long-term recordings we found that in some cases MV treatment led to strong changes of the apparent ratio recorded for both roGFP2-based probes *in vivo* even though the individual channels showed little change. Although we cannot fully explain the exact kinetics of the fluorescence ratio recorded over several hours after MV treatment, we show that the reported effects of MV and light are reliable and reproducible. In addition, inhibitor treatments confirmed that the observed effects are causally connected to primary oxidation occurring in the respective subcellular compartments.

Treatment of seedlings with MV without additional illumination caused oxidation in chloroplasts, and to a minor extent in mitochondria and the cytosol. This contrasts with earlier measurements in which MV caused a minor oxidation in mitochondria and a pronounced oxidation in the cytosol of Arabidopsis cotyledons (Schwarzländer et al., 2009). A major difference between the two experiments is the use of a confocal microscope with laser excitation targeting a small number of cells by Schwarzländer et al. (2009), while a

plate reader with less intense excitation light collecting fluorescence from whole seedlings was used in this work. In the first 2 h after MV addition, the response of the roGFP2-Orp1 sensor was faster and more pronounced compared to Grx1-roGFP2 in plastids or roGFP2-Grx1 in mitochondria, which indicates an increase of H_2O_2 before a change in E_{GSH}. However, because the oxidized roGFP2-Orp1 depends on GSH for its reduction and because the roGFP2 domain may on its own react with GSH/GSSG, a gradual change in sensor oxidation may also reflect changes in the E_{GSH}. If both sensors react to imposed stress (i.e. 5 h after MV addition) it is thus not possible to dissect whether the observed oxidation is caused by H_2O_2 production or an increase of E_{GSH} (Meyer and Dick, 2010; Nietzel et al., 2019). We observed complete oxidation of plastid-targeted roGFP2-Orp1 and partial oxidation of plastid-targeted Grx1-roGFP2 after MV addition, indicating that the excitation light in the plate reader is still sufficient to trigger electron flux in the pETC and hence the formation of ROS (Supplemental Fig. S5). The MV-induced oxidation was considerably slower than the oxidation induced by incubation of seedlings in H_2O_2 (Fig. 3), in accordance with only intermittent illumination during plate reader measurements. The minor oxidation observed for cytosolic sensors after MV challenge indicates that either low amounts of ROS are leaving the chloroplasts under these conditions, or that the capacity of the cytosolic scavenging systems is sufficient to detoxify the H_2O_2 leaking from chloroplasts. H_2O_2 produced in chloroplasts may be detoxified locally through the glutathione–ascorbate cycle. The E_{GSH} in each compartment is independent and not directly correlated (Marty et al., 2019). The resultant GSSG is contained within the organelles, leading to a local change in E_{GSH} to less reducing values. The lethal phenotypes of Arabidopsis mutants deficient in plastidic GR2 strongly suggest that GSSG cannot be efficiently exported from plastids (Marty et al., 2019). In addition, stromal E_{GSH} responds dynamically to light (Haber and Rosenwasser, 2020; Müller-Schüssele et al., 2020) and GSSG can be formed via several enzymes directly or indirectly involved in ROS scavenging (DHAR, GRX, PrxII, MSRB, among others), and its efficiently recycled by GR2.

ROS as a putative mobile signal between cellular sub-compartments

In photosynthetic organisms, light exposure triggers activation or inactivation of multiple redox-regulated enzymes containing thiol-switches (Cejudo et al., 2019). In addition, 20–60 seconds of light stress in Arabidopsis leads to an increase in GSH and total glutathione through processes associated with high levels of nitric oxide and photorespiratory

421 processes providing increased amounts of GSH precursors (Choudhury et al., 2018). From
422 high light treatments of plants transiently expressing HyPer it was deduced that oxidation in
423 plastids and the nucleus takes less than one second (Exposito-Rodriguez et al., 2017). In our
424 experiments, we show a change in the oxidation of sensors targeted to plastids and
425 mitochondria in plants exposed to light (Fig. 4A–B G–H, green curves), indicating that light
426 exposition changes the redox homeostasis in these compartments. Further research will be
427 needed to increase the time resolution of these light-induced redox changes, especially using
428 pH-insensitive sensors such as roGFP2-Orp1 and Grx1-roGFP2, since pH adjustments may
429 be challenging for fast events.

430 Light exposure of samples pre-treated with MV increased the oxidation in
431 chloroplasts, cytosol and mitochondria more than MV alone (Fig. 4), in accordance with
432 enhanced MV toxicity due to pETC activation (Cui et al., 2019). Oxidation of the Grx1-
433 roGFP2 and roGFP2-Grx1 in all compartments was dependent on the pETC, as it was
434 inhibited by DCMU. This was the same for roGFP-Orp1 targeted to cytosol and
435 mitochondria, while only a minor inhibition was observed in plastids (Fig. 5C, E, G). This
436 may indicate that the concentration of DCMU used still allows H_2O_2 production in the
437 chloroplast or that it enhances the production of peroxides through production of singlet
438 oxygen (Fufezan et al., 2002; Krieger-Liszkay, 2005; Dietz et al., 2016). In this same sensor
439 line, no oxidation peak was observed immediately after light exposure (Fig. 4). This peak
440 might have been missed due to a slightly slower transfer of the well plate back into the plate
441 reader.

442 The oxidation of roGFP2-Orp1 in mitochondria after light and MV treatment was
443 dependent on pETC activity, as it was inhibited by DCMU (Fig. 4G, right panel). This
444 indicates that ROS produced in the chloroplast is escaping the local scavenging system and
445 affects redox homeostasis in the cytosol and mitochondria. In high-light stress conditions, the
446 association between plastids and nucleus increases (Exposito-Rodriguez et al., 2017),
447 potentially fostering a direct transfer of ROS from the plastids to the nucleus. Chloroplastic
448 H_2O_2 is believed to act as a secondary messenger involved in retrograde signalling to the
449 nucleus (Chan et al., 2016), where it can modulate the transcriptome (Sewelam et al., 2014).
450 As an example, the over-excitation of PSI can lead to ROS-induced changes in the redox
451 state of antioxidant-related transcription factors such as ZAT10 (Rossel et al., 2007) and
452 HSFA1D, the latter can enhance the expression of the peroxidase AXP2 (Jung et al., 2013).

453 The transfer of ROS from plastids to the cytosol might be facilitated by aquaporins
454 (Mubarakshina et al., 2010). In mammals, Aqp8 and Aqp11 have been already characterized
455 as essential ROS transporters from mitochondria and the endoplasmic reticulum, respectively
456 (Chauvigné et al., 2015; Bestetti et al., 2020). In tobacco chloroplasts, the aquaporin NtAQP1
457 has been described as a gas pore for CO_2 (Uehlein et al., 2008), while plant mitochondria
458 harbour at least 1 aquaporin, TTIP5;1, which is still uncharacterized (Bienert and Chaumont,
459 2014). Dynamic recording of ROS formed at the chloroplastic and mitochondrial ETCs and
460 downstream oxidative changes in other subcellular compartments as established in this work
461 presents opportunities for future research regarding the role of aquaporins in facilitating ROS
462 diffusion across membranes.

463 In mammals and other non-photosynthetic organisms, mitochondria constitute the
464 main source of ROS production under MV treatments (Cochemé and Murphy, 2008). Our
465 findings showed mild oxidation in the mitochondrial matrix after addition of MV (Fig. 3G–I),
466 which can also be observed in the fluorescence intensity shifts of both individual channels at
467 the moment of MV addition to seedlings expressing the mitochondria-targeted roGFP2-Orp1
468 (Supplemental figure S4F, supplemental figure S5F). This initial oxidative shift even before
469 the light treatment was inhibited in plants pre-treated with the mETC inhibitor rotenone but
470 not with the pETC inhibitor DCMU (Fig. 5H, right panels). This indicates that MV-toxicity
471 in mitochondria is independent from the chloroplastic pETC. Notably, rotenone also inhibited
472 the response of E_{GSH} to light/MV treatment in plastids and the cytosol (Fig. 5D, F, left
473 panels). In isolated barley thylakoids rotenone inhibits a NAD(P)H dehydrogenase-like
474 enzyme (NDH) which is implicated in cyclic electron transport via photosynthetic complex I
475 (Teicher and Scheller, 1998). Despite its original name, NDH has been recently shown to
476 preferentially accept electrons from ferredoxin rather than NADPH (Schuller et al., 2019).
477 The key role of NDH in cyclic electron transport may nevertheless explain a direct
478 modulation of light-induced MV toxicity by rotenone. In addition, mitochondria and
479 chloroplasts are metabolically coupled (Schöttler and Tóth, 2014; Shameer et al., 2019).
480 Therefore, we cannot discard an indirect inhibition of the pETC by decreasing the mETC
481 with rotenone.

482 Efficient inhibition of the mETC with rotenone and the pETC with DCMU led to
483 concomitant abolishment of MV-induced changes in both sensors. This observation further
484 supports the notion that the responses of both probes are causally connected to the activity of

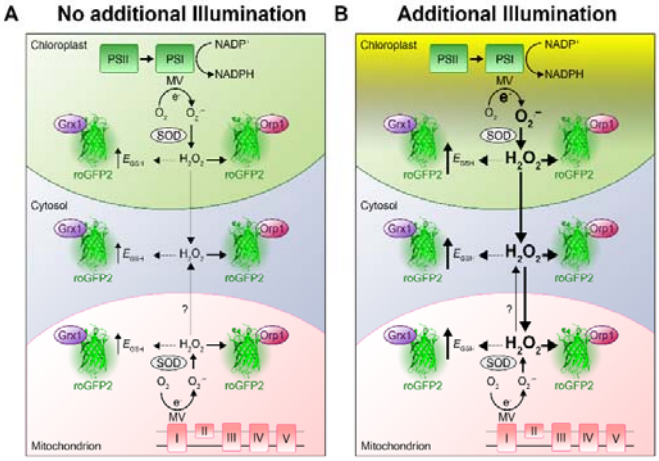

Figure 6. Increased chloroplast-derived ROS production caused by MV modulates the glutathione redox potential in chloroplasts, cytosol and mitochondria. A, MV is an herbicide that causes photo-oxidative stress in chloroplasts by diverting electrons from the photosystem I (PSI) to molecular oxygen (O_2), leading to formation of superoxide ($O_2^{\bullet-}$). In addition, MV is able to transfer electrons from complex I of the mitochondrial electron transport chain to O_2, also generating $O_2^{\bullet-}$. Superoxide is dismutated to H_2O_2 by chloroplastic or mitochondrial superoxide dismutases (SODs). Increased accumulation of H_2O_2 can lead to oxidation of the glutathione buffer, most likely via detoxification along the glutathione–ascorbate cycle (not shown). **B**, Additional light enhances electron transport in the chloroplasts, inducing the production of $O_2^{\bullet-}$ and in consequence also H_2O_2. If the scavenging capacities of the chloroplast are surpassed, H_2O_2 might be leaking to the cytosol and mitochondria. H_2O_2 can indirectly increase local E_{GSH}, which can be tracked using Grx1-roGFP2. The increase of H_2O_2 can be tracked using the oxidation of the roGFP2-Orp1 sensor.

485 either ETCs. The interpretation of alterations in roGFP2 fluorescence as a measure of
486 oxidative responses linked to deviations of electrons from the ETCs thus appears valid (Fig.
487 6). Similarly, inhibitor-dependent abolishment of oxidation in the cytosol caused by MV in

conjunction with light strongly suggests that the observed cytosolic alterations mirror the release of ROS from chloroplasts into the cytosol and mitochondria. With the respective probes and the plate reader setup it is thus possible to measure the immediate and dynamic oxidative response to a stress imposed on chloroplast, in the cytosol and mitochondria. Pulsed short-term stresses like e.g. short periods of strong illumination are followed by a recovery phase. Only if the stress occurs at higher frequencies or even persist permanently, this results in a long-term oxidation.

Concluding remarks

In this work, we have established a simple semi high-throughput approach to follow the contribution of different subcellular compartments to a ROS-mediated oxidation response in living tissues for multiple seedlings and treatment regimes in parallel. The results identify chloroplasts as the principal source of ROS in response to MV in illuminated, photosynthetically active tissue but also highlight the contribution of mitochondria to MV toxicity within plant cells. The ability to record dynamic redox-related changes will pave the way to better understand the interplay between redox imbalances in distinct plant compartments. In future experiments, measuring coupled redox dynamics in combination with genetics will enable further dissection of the signalling events between subcellular compartments.

MATERIALS AND METHODS

Plant material and growth conditions

Arabidopsis thaliana Col-0 ([L.] Heynh.) plants were obtained from NASC (www.arabidopsis.info). Transgenic Col-0 lines expressing the Grx1-roGFP2 sensor in the cytosol have been described earlier by (Marty et al., 2009). For targeting Grx1-roGFP2 to plastids, the sensor construct was cloned behind the target peptide of transketolase (TK_{TP}) (Wirtz and Hell, 2003; Schwarzländer et al., 2008; Speiser et al., 2018). For measurements of E_{GSH} in the mitochondrial matrix, Col-0 plants were transformed with roGFP2-Grx1 cloned behind the target peptide of serine hydroxymethyltransferase ($SHMT_{TP}$) as reported in (Albrecht et al., 2014) and (Marty et al., 2019). Cytosolic and mitochondrial targeted versions of the roGFP2-Orp1 sensor were previously reported (Nietzel et al., 2019), while the plant line expressing the plastid localized version of the sensor was generated in this work. For

experiments with whole seedlings, seeds were surface-sterilized with 70% (v/v) ethanol, rinsed 3 times with sterile deionized water and stratified for 48 h at 4ºC. Seeds were then sown on plates with 0.5x Murashige and Skoog growth medium (Murashige and Skoog, 1962) (Duchefa Biochemie, Haarlem, The Netherlands) supplemented with 0.1% (w/v) sucrose, 0.05% (w/v) MES (pH 5.8, KOH) and 0.8% (w/v) agar. Plates were incubated vertically in a growth chamber under a long-day regime (16 h light, 22 ± 2ºC; 8 h dark 18 ± 2ºC) with a photon flux density of 100 µmol m^{-2} s^{-1} for 7 days.

Cloning of plastid-targeted roGFP2-Orp1 sensor and generation of transgenic plant lines

The roGFP2-Orp1 sequence was amplified by PCR from pBSSK:roGFP2-Orp1 (Gutscher et al., 2009) and fused to TK_{TP}(as described in (Nietzel et al., 2019). Primers for roGFP2-Orp1 amplification were AACCATAGAGAAAACTGAGACTGCGGTGAGCAAGGGCGAGGAGCTGTTC and GTACAAGAAAGCTGGGTTCTATTCCACCTCTTTCAAAAGTTCTTC and for amplification of the targeting peptide TACAAAAAAGCAGGCTTCACCATGGCGTCTTCTTCTTCTCTCACT and GAACAGCTCCTCGCCCTTGCTCACCGCAGTCTCAGTTTTCTCTATGGTT. Fusion of both constructs was achieved by amplification with the primers GGGGACAAGTTTGTACAAAAAAGCAGGCTTCACC and GGGGACCACTTTGTACAAGAAAGCTGGGTTCTA. For constitutive plant expression (CaMV 35S promoter), the amplicon was cloned into pDONR207 (Invitrogen Ltd, Carlsbad, CA) and then into pH2GW7 (Karimi et al., 2002) using Gateway cloning (Invitrogen Ltd, Carlsbad, CA).

Confirmation of subcellular roGFP2 targeting by confocal microscopy

Seven-day-old seedlings were imaged using a confocal laser scanning microscope (Zeiss LSM 780, connected to an Axio Observer.Z1; Carl Zeiss Microscopy, Jena, Germany) with a 40x lens (C-Apochromat 40x/1.2 W Korr). GFP and chlorophyll fluorescence were measured by excitation at 488 nm and emission at 505-530 nm (GFP) and 650–695 nm (chlorophyll). For mitochondrial counter staining, seedlings were vacuum infiltrated for 30 min on 200 nM MitoTracker Orange (Thermo Fisher Scientific, Waltham, MA) and measured by excitation at 543 nm and emission at 570–623 nm.

549 **Purification of recombinant roGFP2 variants**

550 *E. coli* HMS174/Origami cells containing the pET30-roGFP2-His vector were cultured in
551 liquid LB medium supplemented with 50 µg mL^{-1} kanamycin at 37ºC to an OD_{600} of 0.6–0.8.
552 roGFP2-His expression and cell lysis were performed as described in (Nietzel et al., 2019).
553 The lysate was centrifuged at 19,000 *g* for 15 min at 4ºC and the supernatant filtered through
554 a sterile filter of 0.45 µm nominal pore size. The filtered fraction was then loaded onto a Ni-
555 NTA HisTrapTM column (GE Healthcare, Little Chalfont, UK) using a peristaltic pump at a
556 flow rate of 1 mL min^{-1}. Proteins were eluted from the column with a 10–200 mM imidazole
557 gradient (100 mM Tris-HCl, pH 8.0, 200 mM NaCl) using an ÄKTA Prime Plus
558 chromatography system (GE Healthcare). Fractions were collected and stored at 4ºC.

559 **Spectral measurement of roGFP2 probe variants *in planta***

560 4–5 seedlings were placed in 250 µL imaging buffer (10 mM MES, 10 mM $MgCl_2$, 10 mM
561 $CaCl_2$, 5 mM KCl, pH 5.8) in transparent Nunc® 96-well plates. Samples were excited at
562 370–496 nm with a step width of 1 nm and the emission collected at 530±5 nm using a
563 CLARIOstar plate reader (BMG Labtech, Offenburg, Germany). To achieve complete
564 reduction or oxidation of the sensor, the imaging buffer was supplemented with either 20 mM
565 1,4-dithiothreitol (DTT) or 100 mM H_2O_2. Non-transformed wild-type seedlings were treated
566 in the same conditions and used to determine the autofluorescence that was subtracted from
567 the fluorescence recorded in roGFP2 lines. The spectral properties of recombinant roGFP2
568 were measured under the same conditions.

569 **Time-resolved ratiometric analysis of probe fluorescence *in planta***

570 All *in planta* measurements for all different probes were conducted in either a CLARIOstar
571 or POLARstar plate reader (BMG Labtech). roGFP2 was excited by a filter-based excitation
572 system at 410±5 nm and 480±5 nm. Fluorescence was collected using either a 530±20 filter
573 for the POLARstar, or a 520±5 nm for the CLARIOstar. The fluorescence ratio was
574 calculated as 410 nm / 480 nm and normalized to the ratio value at 0 h. Seedlings were
575 treated with different concentrations of H_2O_2 in a final volume of 250 µL imaging buffer. To
576 induce oxidative stress in seedlings by endogenous ROS production, MV (Sigma-Aldrich,
577 Steinheim, Germany) was added at different final concentrations using the built-in automated
578 injectors. Actinic light treatments were performed by placing the plate with seedlings pre-

exposed to MV for 2 h under white LEDs with a photon flux density of 200 µmol m^{-2} s^{-1} for 1 h. Subsequently, the recording of roGFP2 fluorescence was continued in the dark (except for the short light flashes required for the measurements) within the plate reader. To assess the dynamic range of the probes *in planta* and for sensor calibration, 20 mM DTT and subsequently 100 mM H_2O_2 were added at the end of each experiment to fully reduce and fully oxidize the sensors. Between these treatments, samples were rinsed twice with imaging buffer. In each experiment, at least 4 technical replicates consisting of 4–5 pooled seedlings per well were used. Each experiment was repeated at least 3 times.

Samples were incubated with inhibitors of chloroplast and mitochondrial ETC prior to the addition of MV. To inhibit photosystem II (PSII), samples were treated with 10 µM 3-(3,4-dichlorophenyl)-1,1-dimethylurea (DCMU) dissolved in ethanol, whereas 50 µM rotenone (Sigma-Aldrich) was dissolved in dimethyl sulfoxide (DMSO) to inhibit complex I of the electron transport chain in mitochondria.

SUPPLEMENTAL MATERIAL

Supplemental Figure S1. Subcellular localization of roGFP2-based probes for E_{GSH} and H_2O_2 in Arabidopsis.

Supplemental Figure S2. Raw fluorescence of Arabidopsis E_{GSH} and H_2O_2 sensors lines compared with non-transformed Col-0 plants.

Supplemental Figure S3. Calibration procedure to determine the dynamic range of the sensor exemplified for cytosolic roGFP2-Orp1.

Supplemental Figure S4. Individual excitation channels of roGFP2 fluorescence upon MV-induced oxidation in planta.

Supplemental Figure S5. Effect of the excitation light on the MV-induced oxidation of the roGFP2-Orp1 sensor.

Supplemental Figure S6. Effect of extended treatment of Arabidopsis seedlings with MV.

Supplemental Figure S7. Individual excitation channels of roGFP2 fluorescence upon light-enhanced MV-induced oxidation in planta.

FIGURE LEGENDS

Figure 1. Subcellular localization and spectral behavior of E_{GSH} and H_2O_2 sensors in Arabidopsis. A–F (left panels), Confocal microscopy images of leaf epidermal cells from 7-day-old seedlings stably expressing Grx1-roGFP2, roGFP2-Grx1 or roGFP2-Orp1 targeted to plastids (**A–B**), cytosol (**C–D**) or mitochondria (**E**–**F**). All images show roGFP2 fluorescence recorded with λex = 488 nm and λem = 505-530 nm. Bars, 50 μm. **A–F (right panels),** Grx1-roGFP2, roGFP2-Grx1 or roGFP2-Orp1 fluorescence excitation spectra for non-treated seedlings (n.t., grey), and after reduction with 20 mM DTT (blue) or oxidation with 100 mM H_2O_2 (red). All spectra were recorded on a plate reader from 7-day-old seedlings with emission at 520±5 nm and using the same gain for all lines. The curves show the mean of the fluorescence in arbitrary units (AU) +SD, with $n \geq 3$ biological replicates, where each replicate is an independent pool of 4–5 seedlings. All spectra were corrected for the autofluorescence measured in non-transformed control seedlings (see Supplemental Fig. S1). The dynamic range (δ) for the maximum change of the fluorescence ratio between the fully oxidized and fully reduced sensor was calculated from the fluorescence collected after sensor excitation at 410 and 480 nm. **G**, Schematic model of roGFP2 structure highlighting the disulfide bond formation upon reversible oxidation. **H**, Excitation spectrum of purified roGFP2 measured under similar conditions as the seedlings. To achieve full reduction and full oxidation, the purified protein was incubated in 10 mM DTT or 10 mM H_2O_2, respectively. Mean +SD, n = 6.

Figure 2. Real-time monitoring of cytosolic Grx1-roGFP2 and roGFP2-Orp1 redox changes upon imposition of oxidative stress *in planta*. **A,** Pools of 7-day-old seedlings (4–5 per well) expressing Grx1-roGFP2 or roGFP2-Orp1 in the cytosol were placed in a 96-well plate. **B,** The redox state of the sensors was measured as the roGFP2 fluorescence after sequential excitation at λex = 410±5 nm and λex = 480±5 nm. Fluorescence was always recorded at λem = 530±20 nm. **C, E,** Time–resolved fluorescence recordings for the two independent channels after addition of 100 mM H_2O_2 at t = 1 h. Both curves are normalized to their initial values before imposed oxidation (dotted lines). **D, F,** Fluorescence ratio values calculated to the original fluorescence in both channels in response to different concentrations of H_2O_2. For control samples only buffer was added. The curves show the mean ratio +SD from $n = 4$ biological replicates, where each replicate is an independent pool of 4–5 seedlings. The ratio values are normalized to the original ratio values before addition

of H_2O_2. The experiment was repeated three times with similar results. Dotted lines in panels D and F indicate minimum and maximum ratio values measured from the same wells at the end of the experiment during incubation in 100 mM H_2O_2 for full oxidation and in 20 mM DTT for full reduction of the probes (see Supplemental Fig. S3).

Figure 3. Real-time monitoring of E_{GSH} and H_2O_2 sensors upon MV-induced oxidation *in planta*. A–I, Seven-day-old seedlings stably expressing Grx1-roGFP2, roGFP-Grx1 or roGFP2-Orp1 targeted to the cytosol, plastids or mitochondria were placed in a 96-well plate with imaging buffer. After 1 h, MV was added to a final concentration indicated in panel A. In control samples (green), only buffer was added to maintain a uniform total buffer volume throughout the experiments. Ratio values were calculated from the fluorescence recorded by sequential excitation of probes at 410±5 nm and 480±5 nm, and normalized to the initial ratio at 0 h. Fluorescence was always recorded at 530±20 nm. Dotted lines indicate ratio values measured from the same wells at the end of each experiment after incubation in 20 mM DTT for full reduction or 100 mM H_2O_2 for full oxidation of the probes. **C**, **F**, **I**, Endpoint ratio values at 6 h extracted from panels A, B, D, E, G and H. Mean ratios +SD, $n \geq 3$ biological replicates, where each replicate is an independent pool of 4–5 seedlings. Different letters indicate statistical differences between ratios after $\log_{10}$ transformation, according to one-way ANOVA with Tukey's multiple comparison test ($P < 0.05$). Data for individual excitation channels are presented in Supplemental Fig. S4.

Figure 4. Light enhances MV-induced oxidation of roGFP2-derived redox sensors. A–I, Seven-day-old seedlings stably expressing the indicated sensor constructs in plastids, in the cytosol or in mitochondria were placed in a 96-well plate with imaging buffer. After 1 h, MV was added to final concentrations of indicated in panel A. Arrows on the x-axes of panels A, B, D, E, G, and H indicate the time points at which data for the bar charts in panels **C**, **F** and **I** were extracted (i.e. before and after illumination). In control samples (green), only buffer was added. Oxidation of the sensors was recorded as the normalized ratio of the fluorescence recorded with excitation at 410±5 nm and 480±5 nm, respectively. Fluorescence was always recorded at 530±20 nm. After a pre-incubation with MV for 2 h, seedlings were intermittently illuminated for 1 h with actinic light (200 µmol m^{-2} s^{-1}) and redox measurements were subsequently resumed for 2 h. Dotted lines indicate ratio values measured from the same wells at the end of the experiment after incubation in 20 mM DTT for full reduction or 100 mM H_2O_2 for full oxidation of the probes. Mean ratios +SD, $n \geq 4$

biological replicates, where each replicate is an independent pool of 4–5 seedlings. Different letters represent statistical differences between ratios after $\log_{10}$ transformation, according to one-way ANOVA with Tukey's multiple comparison test ($P < 0.05$). Data for individual channels can be found in Supplemental Fig. S7.

Figure 5. Contribution of chloroplast and mitochondrial ETCs to MV-induced oxidation. A, Model depicting the function and interplay of MV and ETC inhibitors on superoxide production in a chloroplast. MV withdraws electrons (e^-) from photosystem I (PSI) and transfers them to molecular oxygen (O_2) to form superoxide ($O_2^{\bullet-}$). DCMU is an inhibitor that specifically blocks electron transfer from photosystem II (PSII) to plastoquinone. **B,** In the mitochondrion, MV is able to transfer electrons from complex I of the mitochondrial electron transport chain to O_2, generating $O_2^{\bullet-}$. Rotenone inhibits complex I activity. **C–H,** Seven-day-old seedlings stably expressing the indicated sensor constructs in plastids, cytosol or mitochondria were placed in 96-well plates with imaging buffer as a control or buffer supplemented with 10 µM DCMU or 50 µM rotenone to inhibit the electron flux along the chloroplastic or mitochondrial ETCs, respectively. After 1 h, MV was added to a final concentration of 50 µM or buffer as a control. After 2 h of treatments, the samples were intermittently exposed to 1 h of actinic light (200 µmol m^{-2} s^{-1}). Data indicate the mean normalized ratio of the sensor fluorescence sequentially excited at 410±5 nm and 480±5 nm, and collected at 530±20 nm in at least four biological replicates (left panels). Arrows on the x-axes of panels C–H indicate the time point at which data for the bar charts (right panels). Dotted lines indicate ratio values measured from the same wells at the end of the experiment during incubation in 20 mM DTT for full reduction or 100 mM H_2O_2 for full oxidation of the probes. Different letters represent statistical differences between ratios after $\log_{10}$ transformation, according to one-way ANOVA with Tukey's multiple comparison test ($P < 0.05$).

Figure 6. Increased chloroplast-derived ROS production caused by MV modulates the glutathione redox potential in chloroplasts, cytosol and mitochondria. A, MV is an herbicide that causes photo-oxidative stress in chloroplasts by diverting electrons from the photosystem I (PSI) to molecular oxygen (O_2), leading to formation of superoxide ($O_2^{\bullet-}$). In addition, MV is able to transfer electrons from complex I of the mitochondrial electron transport chain to O_2, also generating $O_2^{\bullet-}$. Superoxide is dismutated to H_2O_2 by chloroplastic or mitochondrial superoxide dismutases (SODs). Increased accumulation of H_2O_2 can lead to

oxidation of the glutathione buffer, most likely via detoxification along the glutathione–ascorbate cycle (not shown). **B,** Additional light enhances electron transport in the chloroplasts, inducing the production of $O_2^{\bullet-}$ and in consequence also H_2O_2. If the scavenging capacities of the chloroplast are surpassed, H_2O_2 might be leaking to the cytosol and mitochondria. H_2O_2 can indirectly increase local E_{GSH}, which can be tracked using Grx1-roGFP2. The increase of H_2O_2 can be tracked using the oxidation of the roGFP2-Orp1 sensor.

Parsed Citations

Albrecht SC, Sobotta MC, Bausewein D, Aller I, Hell R, Dick TP, Meyer AJ (2014) Redesign of genetically encoded biosensors for monitoring mitochondrial redox status in a broad range of model eukaryotes. J Biomol Screen 19: 379–386
Pubmed: Author and Title
Google Scholar: Author Only Title Only Author and Title

Attacha S, Solbach D, Bela K, Moseler A, Wagner S, Schwarzländer M, Aller I, Müller SJ, Meyer AJ (2017) Glutathione peroxidase-like enzymes cover five distinct cell compartments and membrane surfaces in Arabidopsis thaliana. Plant Cell Environ 40: 1281–1295
Pubmed: Author and Title
Google Scholar: Author Only Title Only Author and Title

Bangash SAK, Müller-Schüssele SJ, Solbach D, Jansen M, Fiorani F, Schwarzländer M, Kopriva S, Meyer AJ (2019) Low-glutathione mutants are impaired in growth but do not show an increased sensitivity to moderate water deficit. PLoS ONE. doi: 10.1371/journal.pone.0220589
Pubmed: Author and Title
Google Scholar: Author Only Title Only Author and Title

Belousov VV, Fradkov AF, Lukyanov KA, Staroverov DB, Shakhbazov KS, Terskikh AV, Lukyanov S (2006) Genetically encoded fluorescent indicator for intracellular hydrogen peroxide. Nat Methods 3: 281–286
Pubmed: Author and Title
Google Scholar: Author Only Title Only Author and Title

Bestetti S, Galli M, Sorrentino I, Pinton P, Rimessi A, Sitia R, Medraño-Fernandez I (2020) Human aquaporin-11 guarantees efficient transport of H2O2 across the endoplasmic reticulum membrane. Redox Biol 28: 101326
Pubmed: Author and Title
Google Scholar: Author Only Title Only Author and Title

Bienert GP, Chaumont F (2014) Aquaporin-facilitated transmembrane diffusion of hydrogen peroxide. Biochim Biophys Acta 1840: 1596–1604
Pubmed: Author and Title
Google Scholar: Author Only Title Only Author and Title

Bilan DS, Belousov VV (2018) In vivo imaging of hydrogen peroxide with HyPer probes. Antioxid Redox Signal 29: 569–584
Pubmed: Author and Title
Google Scholar: Author Only Title Only Author and Title

Boisson-Dernier A, Lituiev DS, Nestorova A, Franck CM, Thirugnanarajah S, Grossniklaus U (2013) ANXUR receptor-like kinases coordinate cell wall integrity with growth at the pollen tube tip via NADPH oxidases. PLoS Biol 11: e1001719
Pubmed: Author and Title
Google Scholar: Author Only Title Only Author and Title

Bratt A, Rosenwasser S, Meyer A, Fluhr R (2016) Organelle redox autonomy during environmental stress. Plant Cell Environ 39: 1909–1919
Pubmed: Author and Title
Google Scholar: Author Only Title Only Author and Title

Caplan JL, Kumar AS, Park E, Padmanabhan MS, Hoban K, Modla S, Czymmek K, Dinesh-Kumar SP (2015) Chloroplast stromules function during innate immunity. Dev Cell 34: 45–57
Pubmed: Author and Title
Google Scholar: Author Only Title Only Author and Title

Cejudo FJ, Ojeda V, Delgado-Requerey V, González M, Pérez-Ruiz JM (2019) Chloroplast redox regulatory mechanisms in plant adaptation to light and darkness. Front Plant Sci 10: 380
Pubmed: Author and Title
Google Scholar: Author Only Title Only Author and Title

Chan KX, Phua SY, Crisp P, McQuinn R, Pogson BJ (2016) Learning the languages of the chloroplast: retrograde signaling and beyond. Annu Rev Plant Biol 67: 25–53
Pubmed: Author and Title
Google Scholar: Author Only Title Only Author and Title

Chauvigné F, Boj M, Finn RN, Cerdà J (2015) Mitochondrial aquaporin-8-mediated hydrogen peroxide transport is essential for teleost spermatozoon motility. Sci Rep 5: 7789
Pubmed: Author and Title
Google Scholar: Author Only Title Only Author and Title

Choudhury FK, Devireddy AR, Azad RK, Shulaev V, Mittler R (2018) Rapid accumulation of glutathione during light stress in Arabidopsis. Plant Cell Physiol 59: 1817–1826
Pubmed: Author and Title
Google Scholar: Author Only Title Only Author and Title

Cochemé HM, Murphy MP (2008) Complex I is the major site of mitochondrial superoxide production by paraquat. J Biol Chem 283: 1786–1798

Pubmed: Author and Title
Google Scholar: Author Only Title Only Author and Title

Costa A, Drago I, Behera S, Zottini M, Pizzo P, Schroeder JI, Pozzan T, Lo Schiavo F (2010) H2O2 in plant peroxisomes: an in vivo analysis uncovers a Ca2+-dependent scavenging system. Plant J Cell Mol Biol 62: 760–772
Pubmed: Author and Title
Google Scholar: Author Only Title Only Author and Title

Cui F, Brosché M, Shapiguzov A, He X-Q, Vainonen JP, Leppälä J, Trotta A, Kangasjärvi S, Salojärvi J, Kangasjärvi J, et al (2019) Interaction of methyl viologen-induced chloroplast and mitochondrial signalling in Arabidopsis. Free Radic Biol Med 134: 555–566
Pubmed: Author and Title
Google Scholar: Author Only Title Only Author and Title

De Col V, Fuchs P, Nietzel T, Elsässer M, Voon CP, Candeo A, Seeliger I, Fricker MD, Grefen C, Møller IM, et al (2017) ATP sensing in living plant cells reveals tissue gradients and stress dynamics of energy physiology. eLife. doi: 10.7554/eLife.26770
Pubmed: Author and Title
Google Scholar: Author Only Title Only Author and Title

Delaunay A, Pflieger D, Barrault MB, Vinh J, Toledano MB (2002) A thiol peroxidase is an H2O2 receptor and redox-transducer in gene activation. Cell 111: 471–481
Pubmed: Author and Title
Google Scholar: Author Only Title Only Author and Title

Dietz K-J, Turkan I, Krieger-Liszkay A (2016) Redox- and reactive oxygen species-dependent signaling into and out of the photosynthesizing chloroplast. Plant Physiol 171: 1541–1550
Pubmed: Author and Title
Google Scholar: Author Only Title Only Author and Title

Dietz K-J, Wesemann C, Wegener M, Seidel T (2019) Toward an integrated understanding of retrograde control of photosynthesis. Antioxid Redox Signal 30: 1186–1205
Pubmed: Author and Title
Google Scholar: Author Only Title Only Author and Title

Erickson JL, Kantek M, Schattat MH (2017) Plastid-nucleus distance alters the behavior of stromules. Front Plant Sci. doi: 10.3389/fpls.2017.01135
Pubmed: Author and Title
Google Scholar: Author Only Title Only Author and Title

Exposito-Rodriguez M, Laissue PP, Yvon-Durocher G, Smirnoff N, Mullineaux PM (2017) Photosynthesis-dependent H2O2 transfer from chloroplasts to nuclei provides a high-light signalling mechanism. Nat Commun 8: 49
Pubmed: Author and Title
Google Scholar: Author Only Title Only Author and Title

Fichman Y, Miller G, Mittler R (2019) Whole-plant live Imaging of reactive oxygen species. Mol Plant 12: 1203–1210
Pubmed: Author and Title
Google Scholar: Author Only Title Only Author and Title

Foyer CH, Noctor G (2005) Redox homeostasis and antioxidant signaling: a metabolic interface between stress perception and physiological responses. Plant Cell 17: 1866–1875
Pubmed: Author and Title
Google Scholar: Author Only Title Only Author and Title

Fricker MD (2016) Quantitative redox imaging software. Antioxid Redox Signal 24: 752–762
Pubmed: Author and Title
Google Scholar: Author Only Title Only Author and Title

Fufezan C, Rutherford AW, Krieger-Liszkay A (2002) Singlet oxygen production in herbicide-treated photosystem II. FEBS Lett 532: 407–410
Pubmed: Author and Title
Google Scholar: Author Only Title Only Author and Title

Gutscher M, Sobotta MC, Wabnitz GH, Ballikaya S, Meyer AJ, Samstag Y, Dick TP (2009) Proximity-based protein thiol oxidation by H2O2-scavenging peroxidases. J Biol Chem 284: 31532–31540
Pubmed: Author and Title
Google Scholar: Author Only Title Only Author and Title

Haber Z, Rosenwasser S (2020) Resolving the dynamics of photosynthetically produced ROS by high-resolution monitoring of chloroplastic EGSH in Arabidopsis. bioRxiv 2020.03.04.976092
Pubmed: Author and Title
Google Scholar: Author Only Title Only Author and Title

Jiang K, Schwarzer C, Lally E, Zhang S, Ruzin S, Machen T, Remington SJ, Feldman L (2006) Expression and characterization of a redox-sensing green fluorescent protein (reduction-oxidation-sensitive green fluorescent protein) in Arabidopsis. Plant Physiol 141: 397–403
Pubmed: Author and Title

Google Scholar: Author Only Title Only Author and Title

Jung H-S, Crisp PA, Estavillo GM, Cole B, Hong F, Mockler TC, Pogson BJ, Chory J (2013) Subset of heat-shock transcription factors required for the early response of Arabidopsis to excess light. Proc Natl Acad Sci U S A 110: 14474–14479

Pubmed: Author and Title
Google Scholar: Author Only Title Only Author and Title

Karimi M, Inzé D, Depicker A (2002) GATEWAY vectors for Agrobacterium-mediated plant transformation. Trends Plant Sci 7: 193–195

Pubmed: Author and Title
Google Scholar: Author Only Title Only Author and Title

Krieger-Liszkay A (2005) Singlet oxygen production in photosynthesis. J Exp Bot 56: 337–346

Pubmed: Author and Title
Google Scholar: Author Only Title Only Author and Title

Liebthal M, Maynard D, Dietz K-J (2018) Peroxiredoxins and redox signaling in plants. Antioxid Redox Signal 28: 609–624

Pubmed: Author and Title
Google Scholar: Author Only Title Only Author and Title

Liu Z-J, Zhang X-L, Bai J-G, Suo B-X, Xu P-L, Wang L (2009) Exogenous paraquat changes antioxidant enzyme activities and lipid peroxidation in drought-stressed cucumber leaves. Sci Hortic 121: 138–143

Pubmed: Author and Title
Google Scholar: Author Only Title Only Author and Title

Mangano S, Denita-Juarez SP, Marzol E, Borassi C, Estevez JM (2018) High auxin and high phosphate impact on RSL2 expression and ROS-homeostasis linked to root hair growth in Arabidopsis thaliana. Front Plant Sci 9: 1164

Pubmed: Author and Title
Google Scholar: Author Only Title Only Author and Title

Marty L, Bausewein D, Müller C, Bangash SAK, Moseler A, Schwarzländer M, Müller-Schüssele SJ, Zechmann B, Riondet C, Balk J, et al (2019) Arabidopsis glutathione reductase 2 is indispensable in plastids, while mitochondrial glutathione is safeguarded by additional reduction and transport systems. New Phytol 224: 1569–1584

Pubmed: Author and Title
Google Scholar: Author Only Title Only Author and Title

Marty L, Siala W, Schwarzländer M, Fricker MD, Wirtz M, Sweetlove LJ, Meyer Y, Meyer AJ, Reichheld J-P, Hell R (2009) The NADPH-dependent thioredoxin system constitutes a functional backup for cytosolic glutathione reductase in Arabidopsis. Proc Natl Acad Sci 106: 9109–9114

Pubmed: Author and Title
Google Scholar: Author Only Title Only Author and Title

Meyer AJ, Brach T, Marty L, Kreye S, Rouhier N, Jacquot J-P, Hell R (2007) Redox-sensitive GFP in Arabidopsis thaliana is a quantitative biosensor for the redox potential of the cellular glutathione redox buffer. Plant J Cell Mol Biol 52: 973–986

Pubmed: Author and Title
Google Scholar: Author Only Title Only Author and Title

Meyer AJ, Dick TP (2010) Fluorescent protein-based redox probes. Antioxid Redox Signal 13: 621–650

Pubmed: Author and Title
Google Scholar: Author Only Title Only Author and Title

Morgan B, Sobotta MC, Dick TP (2011) Measuring EGSH and H2O2 with roGFP2-based redox probes. Free Radic Biol Med 51: 1943–1951

Pubmed: Author and Title
Google Scholar: Author Only Title Only Author and Title

Morgan B, Van Laer K, Owusu TNE, Ezeriņa D, Pastor-Flores D, Amponsah PS, Tursch A, Dick TP (2016) Real-time monitoring of basal H2O2 levels with peroxiredoxin-based probes. Nat Chem Biol 12: 437–443

Pubmed: Author and Title
Google Scholar: Author Only Title Only Author and Title

Mubarakshina MM, Ivanov BN, Naydov IA, Hillier W, Badger MR, Krieger-Liszkay A (2010) Production and diffusion of chloroplastic H2O2 and its implication to signalling. J Exp Bot 61: 3577–3587

Pubmed: Author and Title
Google Scholar: Author Only Title Only Author and Title

Müller SM, Galliardt H, Schneider J, Barisas BG, Seidel T (2013) Quantification of Förster resonance energy transfer by monitoring sensitized emission in living plant cells. Front Plant Sci 4: 413

Pubmed: Author and Title
Google Scholar: Author Only Title Only Author and Title

Müller-Schüssele SJ, Wang R, Gütle DD, Romer J, Rodriguez-Franco M, Scholz M, Buchert F, Lüth VM, Kopriva S, Dörmann P, et al (2020) Chloroplasts require glutathione reductase to balance reactive oxygen species and maintain efficient photosynthesis. Plant J. doi: 10.1111/tpj.14791

Pubmed: Author and Title
Google Scholar: Author Only Title Only Author and Title

Murashige T, Skoog F (1962) A revised medium for rapid growth and bio assays with tobacco tissue cultures. Physiol Plant 15: 473–497
Pubmed: Author and Title
Google Scholar: Author Only Title Only Author and Title

Narendra S, Venkataramani S, Shen G, Wang J, Pasapula V, Lin Y, Kornyeyev D, Holaday AS, Zhang H (2006) The Arabidopsis ascorbate peroxidase 3 is a peroxisomal membrane-bound antioxidant enzyme and is dispensable for Arabidopsis growth and development. J Exp Bot 57: 3033–3042
Pubmed: Author and Title
Google Scholar: Author Only Title Only Author and Title

Nietzel T, Elsässer M, Ruberti C, Steinbeck J, Ugalde JM, Fuchs P, Wagner S, Ostermann L, Moseler A, Lemke P, et al (2019) The fluorescent protein sensor roGFP2-Orp1 monitors in vivo H2O2 and thiol redox integration and elucidates intracellular H2O2 dynamics during elicitor-induced oxidative burst in Arabidopsis. New Phytol 221: 1649–1664
Pubmed: Author and Title
Google Scholar: Author Only Title Only Author and Title

Pak VV, Ezeriņa D, Lyublinskaya OG, Pedre B, Tyurin-Kuzmin PA, Mishina NM, Thauvin M, Young D, Wahni K, Gache SAM, et al (2020) Ultrasensitive genetically encoded indicator for hydrogen peroxide identifies roles for the oxidant in cell migration and mitochondrial function. Cell Metab 31: 642-653.e6
Pubmed: Author and Title
Google Scholar: Author Only Title Only Author and Title

Park S-W, Li W, Viehhauser A, He B, Kim S, Nilsson AK, Andersson MX, Kittle JD, Ambavaram MMR, Luan S, et al (2013) Cyclophilin 20-3 relays a 12-oxo-phytodienoic acid signal during stress responsive regulation of cellular redox homeostasis. Proc Natl Acad Sci U S A 110: 9559–9564
Pubmed: Author and Title
Google Scholar: Author Only Title Only Author and Title

Pérez-Sancho J, Tilsner J, Samuels AL, Botella MA, Bayer EM, Rosado A (2016) Stitching organelles: organization and function of specialized membrane contact sites in plants. Trends Cell Biol 26: 705–717
Pubmed: Author and Title
Google Scholar: Author Only Title Only Author and Title

Perico C, Sparkes I (2018) Plant organelle dynamics: cytoskeletal control and membrane contact sites. New Phytol 220: 381–394
Pubmed: Author and Title
Google Scholar: Author Only Title Only Author and Title

Queval G, Hager J, Gakière B, Noctor G (2008) Why are literature data for H2O2 contents so variable? A discussion of potential difficulties in the quantitative assay of leaf extracts. J Exp Bot 59: 135–146
Pubmed: Author and Title
Google Scholar: Author Only Title Only Author and Title

Rodrigues O, Reshetnyak G, Grondin A, Saijo Y, Leonhardt N, Maurel C, Verdoucq L (2017) Aquaporins facilitate hydrogen peroxide entry into guard cells to mediate ABA- and pathogen-triggered stomatal closure. Proc Natl Acad Sci U S A 114: 9200–9205
Pubmed: Author and Title
Google Scholar: Author Only Title Only Author and Title

Rosenwasser S, Rot I, Meyer AJ, Feldman L, Jiang K, Friedman H (2010) A fluorometer-based method for monitoring oxidation of redox-sensitive GFP (roGFP) during development and extended dark stress. Physiol Plant 138: 493–502
Pubmed: Author and Title
Google Scholar: Author Only Title Only Author and Title

Rosenwasser S, Rot I, Sollner E, Meyer AJ, Smith Y, Leviatan N, Fluhr R, Friedman H (2011) Organelles contribute differentially to reactive oxygen species-related events during extended darkness. Plant Physiol 156: 185–201
Pubmed: Author and Title
Google Scholar: Author Only Title Only Author and Title

Rossel JB, Wilson PB, Hussain D, Woo NS, Gordon MJ, Mewett OP, Howell KA, Whelan J, Kazan K, Pogson BJ (2007) Systemic and Intracellular Responses to Photooxidative Stress in Arabidopsis. Plant Cell 19: 4091–4110
Pubmed: Author and Title
Google Scholar: Author Only Title Only Author and Title

Scarpeci TE, Zanor MI, Carrillo N, Mueller-Roeber B, Valle EM (2008) Generation of superoxide anion in chloroplasts of Arabidopsis thaliana during active photosynthesis: a focus on rapidly induced genes. Plant Mol Biol 66: 361–378
Pubmed: Author and Title
Google Scholar: Author Only Title Only Author and Title

Schöttler MA, Tóth SZ (2014) Photosynthetic complex stoichiometry dynamics in higher plants: environmental acclimation and photosynthetic flux control. Front Plant Sci 5: 188
Pubmed: Author and Title
Google Scholar: Author Only Title Only Author and Title

Schuller JM, Birrell JA, Tanaka H, Konuma T, Wulfhorst H, Cox N, Schuller SK, Thiemann J, Lubitz W, Sétif P, et al (2019) Structural adaptations of photosynthetic complex I enable ferredoxin-dependent electron transfer. Science 363: 257–260

Pubmed: Author and Title
Google Scholar: Author Only Title Only Author and Title

Schwarzländer M, Dick TP, Meyer AJ, Morgan B (2016) Dissecting redox biology using fluorescent protein sensors. Antioxid Redox Signal 24: 680–712
Pubmed: Author and Title
Google Scholar: Author Only Title Only Author and Title

Schwarzländer M, Fricker MD, Müller C, Marty L, Brach T, Novak J, Sweetlove LJ, Hell R, Meyer AJ (2008) Confocal imaging of glutathione redox potential in living plant cells. J Microsc 231: 299–316
Pubmed: Author and Title
Google Scholar: Author Only Title Only Author and Title

Schwarzländer M, Fricker MD, Sweetlove LJ (2009) Monitoring the in vivo redox state of plant mitochondria: effect of respiratory inhibitors, abiotic stress and assessment of recovery from oxidative challenge. Biochim Biophys Acta 1787: 468–475
Pubmed: Author and Title
Google Scholar: Author Only Title Only Author and Title

Schwarzländer M, Wagner S, Ermakova YG, Belousov VV, Radi R, Beckman JS, Buettner GR, Demaurex N, Duchen MR, Forman HJ, et al (2014) The "mitoflash" probe cpYFP does not respond to superoxide. Nature 514: E12-14
Pubmed: Author and Title
Google Scholar: Author Only Title Only Author and Title

Sewelam N, Jaspert N, Van Der Kelen K, Tognetti VB, Schmitz J, Frerigmann H, Stahl E, Zeier J, Van Breusegem F, Maurino VG (2014) Spatial H2O2 signaling specificity: H2O2 from chloroplasts and peroxisomes modulates the plant transcriptome differentially. Mol Plant 7: 1191–1210
Pubmed: Author and Title
Google Scholar: Author Only Title Only Author and Title

Shameer S, Ratcliffe RG, Sweetlove LJ (2019) Leaf energy balance requires mitochondrial respiration and export of chloroplast NADPH in the light. Plant Physiol 180: 1947–1961
Pubmed: Author and Title
Google Scholar: Author Only Title Only Author and Title

Shapiguzov A, Vainonen JP, Hunter K, Tossavainen H, Tiwari A, Järvi S, Hellman M, Aarabi F, Alseekh S, Wybouw B, et al (2019) Arabidopsis RCD1 coordinates chloroplast and mitochondrial functions through interaction with ANAC transcription factors. eLife. doi: 10.7554/eLife.43284
Pubmed: Author and Title
Google Scholar: Author Only Title Only Author and Title

Smirnoff N, Arnaud D (2019) Hydrogen peroxide metabolism and functions in plants. New Phytol 221: 1197–1214
Pubmed: Author and Title
Google Scholar: Author Only Title Only Author and Title

Sobotta MC, Barata AG, Schmidt U, Mueller S, Millonig G, Dick TP (2013) Exposing cells to H2O2: a quantitative comparison between continuous low-dose and one-time high-dose treatments. Free Radic Biol Med 60: 325–335
Pubmed: Author and Title
Google Scholar: Author Only Title Only Author and Title

de Souza A, Wang J-Z, Dehesh K (2017) Retrograde signals: integrators of interorganellar communication and orchestrators of plant development. Annu Rev Plant Biol 68: 85–108
Pubmed: Author and Title
Google Scholar: Author Only Title Only Author and Title

Speiser A, Silbermann M, Dong Y, Haberland S, Uslu VV, Wang S, Bangash SAK, Reichelt M, Meyer AJ, Wirtz M, et al (2018) Sulfur partitioning between glutathione and protein synthesis determines plant growth. Plant Physiol 177: 927–937
Pubmed: Author and Title
Google Scholar: Author Only Title Only Author and Title

Sylvestre-Gonon E, Law SR, Schwartz M, Robe K, Keech O, Didierjean C, Dubos C, Rouhier N, Hecker A (2019) Functional, structural and biochemical features of plant serinyl-glutathione transferases. Front Plant Sci. doi: 10.3389/fpls.2019.00608
Pubmed: Author and Title
Google Scholar: Author Only Title Only Author and Title

Teicher BH, Scheller VH (1998) The NAD(P)H dehydrogenase in barley thylakoids is photoactivatable and uses NADPH as well as NADH. Plant Physiol 117: 525–532
Pubmed: Author and Title
Google Scholar: Author Only Title Only Author and Title

Uehlein N, Otto B, Hanson DT, Fischer M, McDowell N, Kaldenhoff R (2008) Function of Nicotiana tabacum aquaporins as chloroplast gas pores challenges the concept of membrane CO2 permeability. Plant Cell 20: 648–657
Pubmed: Author and Title
Google Scholar: Author Only Title Only Author and Title

Ugalde JM, Lamig L, Herrera-Vásquez A, Fuchs P, Müller-Schüssele SJ, Meyer AJ, Holuigue L (2020) GSTU7 affects growth

performance and acts as an antagonist of oxidative stress induced by methyl viologen. bioRxiv 2020.06.09.142729
Pubmed: Author and Title
Google Scholar: Author Only Title Only Author and Title

Van Aken O, Ford E, Lister R, Huang S, Millar AH (2016) Retrograde signalling caused by heritable mitochondrial dysfunction is partially mediated by ANAC017 and improves plant performance. Plant J Cell Mol Biol 88: 542–558
Pubmed: Author and Title
Google Scholar: Author Only Title Only Author and Title

Wagner S, Steinbeck J, Fuchs P, Lichtenauer S, Elsässer M, Schippers JHM, Nietzel T, Ruberti C, Van Aken O, Meyer AJ, et al (2019) Multiparametric real-time sensing of cytosolic physiology links hypoxia responses to mitochondrial electron transport. New Phytol 224: 1668–1684
Pubmed: Author and Title
Google Scholar: Author Only Title Only Author and Title

Waszczak C, Carmody M, Kangasjärvi J (2018) Reactive oxygen species in plant signaling. Annu Rev Plant Biol 69: 209–236
Pubmed: Author and Title
Google Scholar: Author Only Title Only Author and Title

Wirtz M, Hell R (2003) Production of cysteine for bacterial and plant biotechnology: application of cysteine feedback-insensitive isoforms of serine acetyltransferase. Amino Acids 24: 195–203
Pubmed: Author and Title
Google Scholar: Author Only Title Only Author and Title